Supporting Information

Driving forces of conformational changes in single-layer graphene oxide

Raymond L.D. Whitby*, Vladimir M. Gun'ko, Alina Korobeinyk, Rosa Busquets, Andrew B. Cundy, Krisztina László, Jadwiga Skubiszewska-Zięba, Roman Leboda, Etelka Tombácz, Ildiko Y. Toth, Krisztina Kovacs, Sergey V. Mikhalovsky

S1. Discussion

Oxidation of carbon materials generates not only oxygen-containing functional groups covalently attached to the surface but also oxidative debris (or fulvic acids) that become adsorbed on graphitic surfaces and can only be removed through extensive washing in a base solution.[1] The oxidative decomposition products of graphenes are expected given that similar observations were observed for acid-oxidized carbon nanotubes,[2] which comprise of graphene sheets. The presence of oxidative debris, which may account for up to 30 % of the total mass of the sample, has a significant effect on the stability of nanocarbon suspensions in aqueous solution. Herein, single layer graphene oxide (SLGO) was cleaned by washing with an alkali solution to ensure removal of fulvic acids from the material, with the regeneration of acidic groups in an acid wash, which is similar to that reported for oxidized CNTs[3].

The single-layer of SLGO was confirmed through atomic force microscopy, which revealed a step height of 0.5 to 0.7 nm corresponding to a single layer. The total number of functional groups (including carboxylic, lactone and phenolic environments on the surface of carbons that are capable of titrating)[4] of SLGO was found to be ca. 7.5 mmol g^{-1}.[5] For a sheet of SLGO, the periphery has a capacity of around 0.3 at% of acidic groups, which implies that the remainder of oxygen-containing groups has to be distributed across both sides of the graphene sheet at around 10 at%. The type and distribution of oxygen-functional groups has also been studied using a variety of techniques including solid state NMR, XPS and micro-

Raman, AFM and STM,[6, 7] *etc*. and the structure of this SLGO appears to conform to that of the Lerf model[8] and in morphology to that of SLGO used elsewhere.[6]

In the absence of acid/base consuming impurities, the net proton consumption in potentiometric titrations is equal to the net proton surface excess amount, which is assigned to the pH-dependent surface charging; its sign indicates the sign of charges formed, and its absolute value equals to the specific amount of negatively charged acidic groups (Fig. S1).

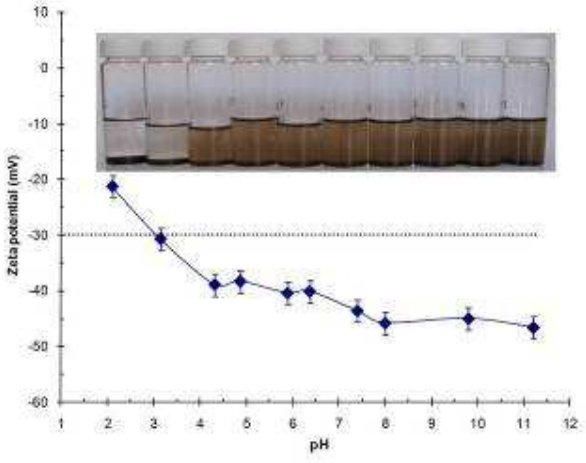

Figure S1. Zeta potential over pH range (SLGO 0.1 mg/L)

As the pH changes from acidic to alkaline, the morphology of the SLGO undergoes a dramatic change and appears more folded through internal collapse of individual sheets (Fig. S2), which might, in addition to the change of surface charge, also account for the better stability of SLGO in aqueous solution at high pH whereas the agglomeration of numerous sheets at low pH causes SLGO to fall instantly out of solution.

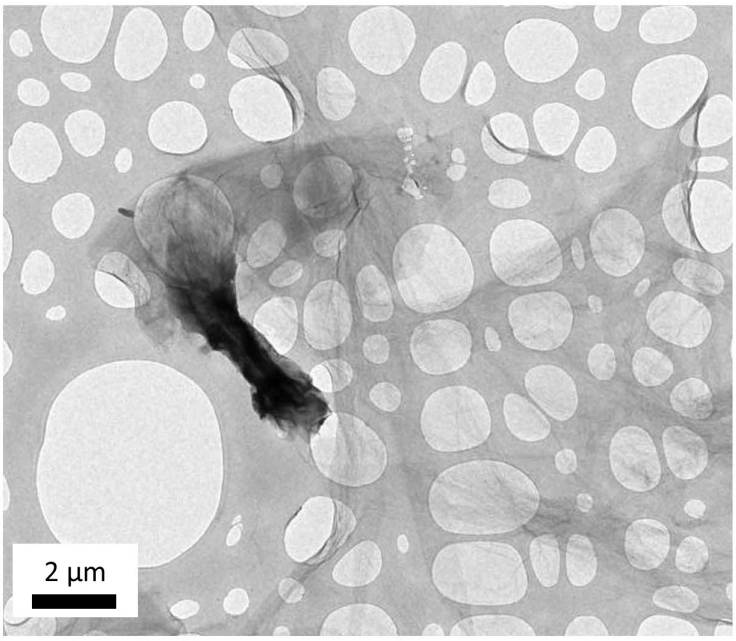

Figure S2. TEM image of SLGO dried from a pH 12 solution.

TGA analysis revealed a 5 % mass loss between 100 and 150 ^{o}C rising to a 28 % mass loss at 250 ^{o}C (Fig. S3). The former is likely due to residual water in the system, whereas the latter is due to loss of functional groups and structural degradation.

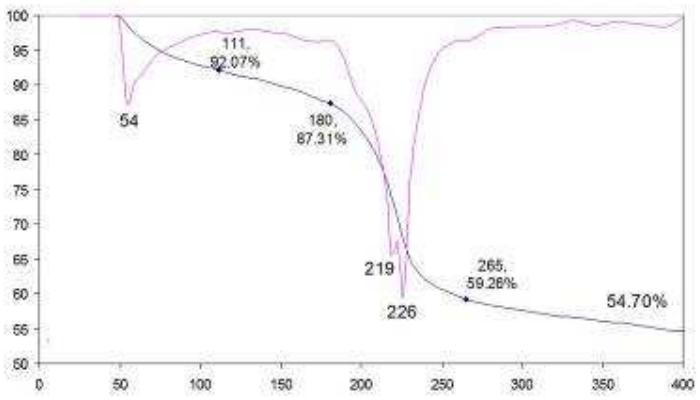

Figure S3. TGA profile of SLGO in nitrogen.

According to theoretical estimations, the specific surface area of single-layer graphene (SLG) composed of single/double carbon sheets can be about 2600-2700 m^2/g,[11] close to the maximum characteristic for carbon materials (approximately 4200 m^2/g, estimated for single-layer nanosheets without formation of stacks). However, the specific surface area, S_{BET} of graphene-like nanosheets determined by low temperature nitrogen adsorption techniques can be much lower, and the nitrogen adsorption-desorption isotherm shape shows that this material comprises agglomerated particles. For instance, the S_{BET} value of few layers graphene systems changes in the range of 270-1550 m^2/g, some of them approaching the S_{BET} value of SLG.

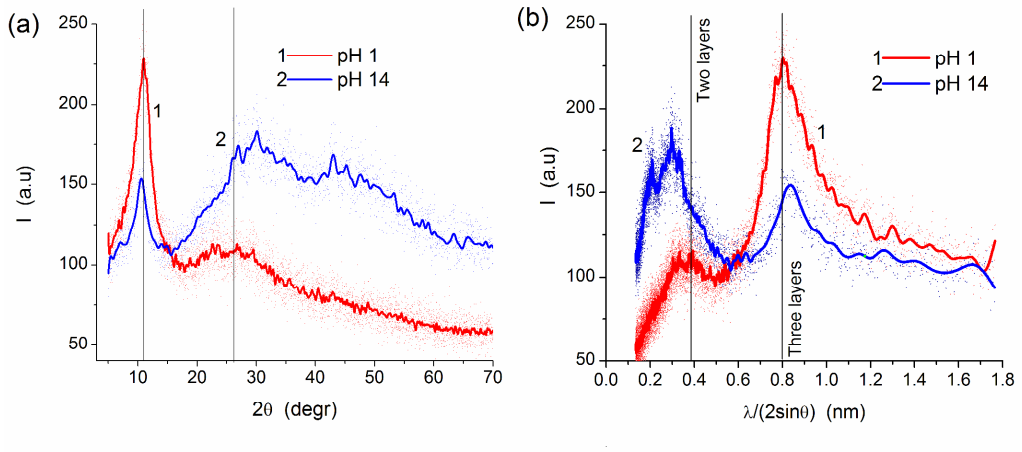

Figure S4. (a) Powder XRD of SLGO suspended at: (1) pH 1 and then dried and (2) pH 14 and then dried, and (b) corresponding d-spacing values with shown boundary values for two and three layer structures.

The XRD pattern of SLGO dried from the suspension at low pH value (Fig. S4a curve 1) reveals a prominent peak at $2\theta \approx 11^o$ giving a *d*-spacing of around 0.8 nm (corresponding to three-layer stacks with removed middle layer) with a minor broader peak centered around 26^o and a *d*-spacing of 0.3 to 0.4 nm (Fig. S4b curve 1) corresponding to few layers stacked in a near or completely nonporous arrangement similar to that in graphite or expanded graphite

having thicker stacks (typically 100-200 nm) compared with aggregated SLGO. The XRD pattern of SLGO dried from the suspension at high pH value (Fig. S4a curve 2) reveals diminution of the 11° peak, an increase of a peak around 28°, and the presence of a low intensity peak at 43° (Fig. S4b curve 2).

Liquid nitrogen adsorption isotherms (Fig. S5) and the resulting pore size distribution profiles were measured for degassed SLGO and compared with SLG,[11] multi-walled carbon nanotubes and expanded graphite. Aggregated SLGO has a major pore fraction at 0.6 nm with minor contributions at 1.3 and 53 nm, which is broadly similar to that of SLG though the latter has a larger contribution at 1.8 nm. Herein, as SLG contains fewer defects, its pore size distribution profiles indicate agglomerated layering or folding within the system. Inflexible graphitic carbon systems, such as expanded graphite, exhibit a series of minor contributing pore sizes with a larger distribution at the higher end, ca. 100 nm, corresponding to voids between relatively thick stacks of sheets and a small portion of the discrete spacing of graphite layers in these stacks. However, multi-walled carbon nanotubes exhibit small pores at 1.8 nm, which are likely due to lattice defects in the walls, and larger pores at 15 and 50 nm, which refer to intertube channels and voids between tubes in their aggregates.

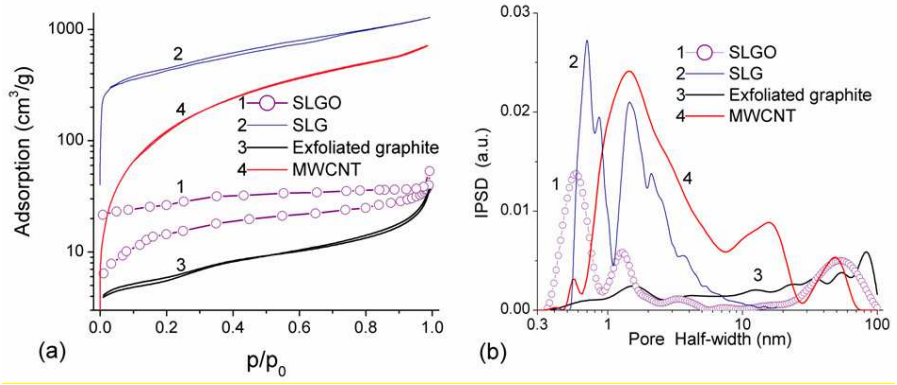

Figure S5. (a) Nitrogen adsorption-desorption isotherms for degassed SLGO (curve 1), SLG (2), exfoliated graphite (3) and multi-walled carbon nanotubes (MWCNTs) (4) (before the measurements SLGO, expanded graphite and MWCNTs were degassed at 150 °C for 2 h);

and (b) incremental PSD calculated using the nitrogen adsorption-desorption isotherms with the DFT method and slit-shaped (SLG, SLGO, exfoliated graphite) and cylindrical (MWCNTs) pore model.

Three structures were selected for SLGO and three structures for SLG, i.e. planar (SLGO-0 – Fig. 1a, SLG-0 – Fig. 1b), strongly bent (SLGO-1 – Fig. 1c, SLG-1 – Fig. 1d) and less bent (SLGO-2 – Fig. 1e, SLG-2 – Fig. 1f) geometries. The geometry of SLGO-0 and SLG-0 was optimized with CharMM force field[12] and then with PM6/MOZYME[13] using a maximum energy gradient per coordinates < 1 kcal/mol/A. For SLGO-1 and SLG-1, the geometry was optimized with CharMM force field and than with PM6/MOZYME maximum energy gradient per coordinates ~ 2 kcal/mol/A with very slow changes in the gradients, i.e. the system is in a local energy minimum. And for SLGO-2 and SLG-2, their geometry was calculated by continue the optimization process with PM6/MOZYME for SLGO-1, SLG-1 to maximum energy gradient per coordinates < 1 kcal/mol/A. The difference in the energy between plane and two folded structures was extrapolated to show the total energy of the SLGO system is lowest for SLGO-2 < SLGO-0 < SLGO-1. However, for the SLG system, this is reversed with the lowest energy for SLG-0 < SLG-2 < SLG-1. This difference shows that folding can occur more easily for SLGO than SLG. Therefore, SLG tends to form stacks through intersheet layering, which is confirmed by the nitrogen isotherm shape with narrow hysteresis loop, whereas SLGO forms more complicated structures and the isotherm of a heated sample has an open hysteresis loop (Fig. S5).

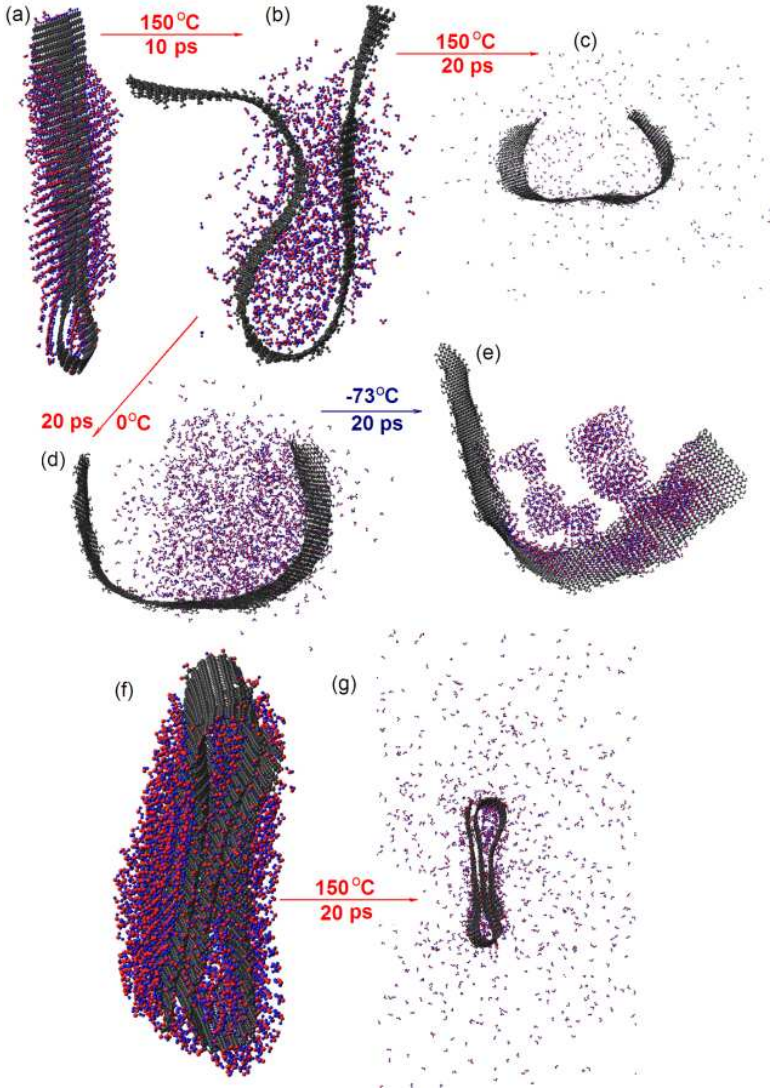

Figure S6. MD (CharMM force field)[12, 14] simulations of (a, f) hydrated folded SLGO under different drying rates and different temperatures: (b, c, g) 150 °C and (d) 0 °C for 20 ps; (e) structure shown in (d) was cooled at 200 K and optimized; structures (a), (e) and (f) are with the optimized geometry; sheet sizes: (a)-(e) 20.8×3.9 nm^2 and (f), (g) 20.9×7.9 nm^2.

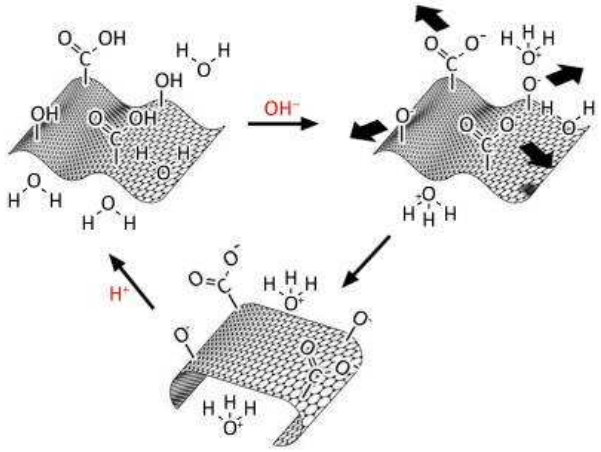

Scheme S1. The conformational changes of an SLGO sheet are caused by the close proximity of oxygen-containing groups on the same side of SLGO (peripheral O-containing groups are not shown). When deprotonation with hydroxide ions of oxygen-containing acidic groups occurs, the repulsion (heavy black arrows) causes the surrounding graphene layer to fold away. When the system is protonated with hydrogen ions, the planar architecture is restored.

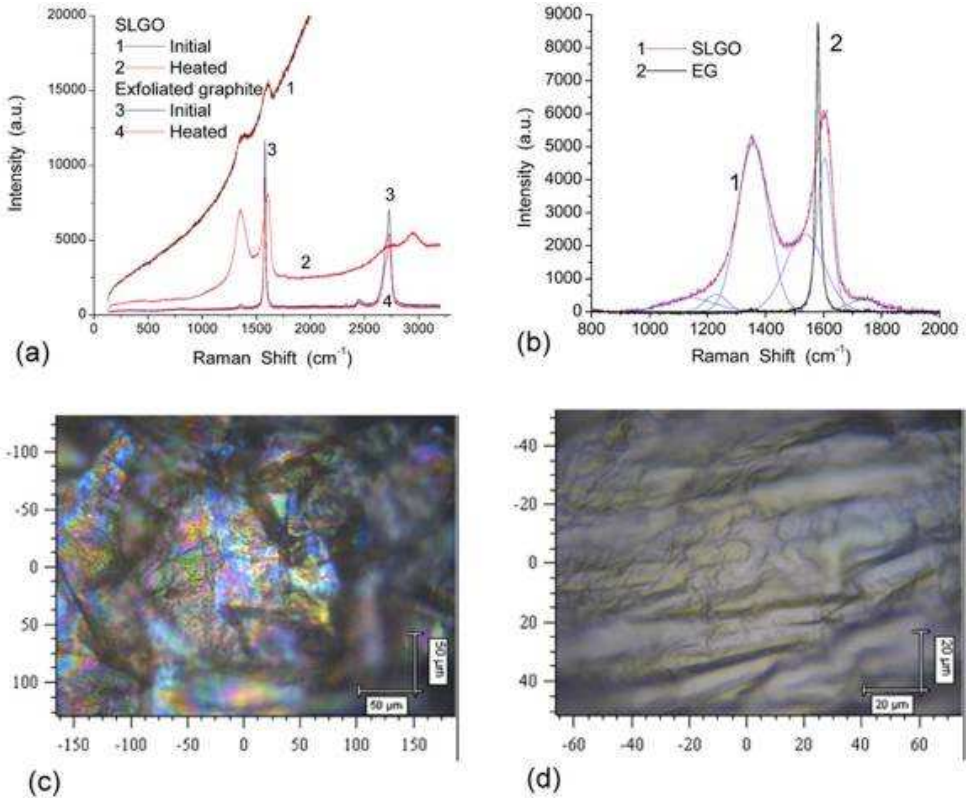

Figure S7. (a) Raman spectra (excitation at 514 nm) of SLGO (1, 2) and exfoliated graphite, EG (3, 4) initial (1, 3) and heated (2, 4) at 150 ^{o}C for 2 h in vacuum, (b) deconvolution of the D and G bands (using the Gaussian functions) of heated SLGO and spectrum of heated EG, and microimages (×500, DMLM Leica microscope) of the SLGO samples (c) initial and (d) degassed/heated.

The Raman spectra also showed sharpening and increase in intensity of the D (sp^3 structures) and G (sp^2 structures) bands (Fig. S7) after SLGO heating, which indicates enhanced sheet-sheet interactions. Raman spectrum of initial SLGO (Fig. S7, curve 1) shows G band at 1600 cm^{-1}, D band at 1352 cm^{-1} and weak second order features observed for heated SLGO sample at 2950 and 2700 cm^{-1}. There is a 5 cm^{-1} blue shift of the G band of SLGO in comparison with that of exfoliated graphite (Fig. S7b). Both D and G bands of heated SLGO are broader than the G band of EG as well as the band of the second order features at 2950 and 2700 cm^{-1}. Changes in the thickness of the heated SLGO structures are reflected in the color changes of images since the initial SLGO has rainbow image (Fig. S7c), but the collapsed structure of heated SLGO is dark grey and opaque (Fig. S7d).

Deconvolution of the spectrum of heated SLGO gives three bands for the D band and three bands for the G band (Fig. S7b). This result can be explained by certain disorder (similar to that observed with XRD method (Fig. S4) in the SLGO sheets and non-graphitic structure of the sheet aggregates because of the presence of many O-containing functionalities distributed over the whole area of the sheets. The SLGO spectrum has a band at 2950 cm^{-1} which is absent in the spectra of exfoliated graphite. This band can be attributed to C-H groups in SLGO. For EG, the D band is very weak in contrast to SLGO, i.e. exfoliated graphite keeps the major portion of the graphitic sp^2 structures.

REFERENCES

1. Rourke, J. P.; Pandey, P. A.; Moore, J. J.; Bates, M.; Kinloch, I. A.; Young, R. J.; Wilson, N. R., The Real Graphene Oxide Revealed: Stripping the Oxidative Debris from the Graphene-like Sheets. *Angew. Chem. Int. Ed.* **2011**, *50*, 3173-3177.

2. Verdejo, R.; Lamoriniere, S.; Cottam, B.; Bismarck, A.; Shaffer, M., Removal of Oxidation Debris from Multi-Walled Carbon Nanotubes. *Chem. Comm.* **2007**, 513-515.

3. Wang, Z. W.; Shirley, M. D.; Meikle, S. T.; Whitby, R. L. D.; Mikhalovsky, S. V., The Surface Acidity of Acid Oxidized Multi-Walled Carbon Nanotubes and the Influence of in-situ Generated Fulvic Acids on their Stability in Aqueous Dispersions. *Carbon* **2009**, *47*, 73-79.

4. Boehm, H. P., Surface Oxides on Carbon and their Analysis: A Critical Assessment. *Carbon* **2002**, *40*, 145-149.

5. Wang, Z.; Korobeinyk, A.; Whitby, R. L. D.; Meikle, S. T.; Mikhalovsky, S. V.; Acquah, S. F. A.; Kroto, H. W., Direct Confirmation that Carbon Nanotubes Still React Covalently after Removal of Acid-Oxidative Lattice Fragments. *Carbon* **2010**, *48*, 916-918.

6. Gao, W.; Alemany, L. B.; Ci, L. J.; Ajayan, P. M., New Insights into the Structure and Reduction of Graphite Oxide. *Nat. Chem.* **2009**, *1*, 403-408.

7. Singh, V.; Joung, D.; Zhai, L.; Das, S.; Khondaker, S. I.; Seal, S., Graphene Based Materials: Past, Present and Future. *Prog. Mater. Sci.* **2011**, *56*, 1178-1271.

8. Lerf, A.; He, H. Y.; Forster, M.; Klinowski, J., Structure of Graphite Oxide Revisited. *J. Phys. Chem. B* **1998**, *102*, 4477-4482.

9. FieldView 2.0.2, www.cresset-group.com, 2011

10. Frisch, M. J.; Trucks, G. W.; Schlegel, H. B.; Scuseria, G. E.; Robb, M. A.; Cheeseman, J. R.; Scalmani, G.; Barone, V.; Mennucci, B.; Petersson, G. A.; *et al.*, Gaussian. *Gaussian Inc., Wallingford CT, USA* 2004.

11. Rao, C. N. R.; Sood, A. K.; Voggu, R.; Subrahmanyam, K. S., Some Novel Attributes of Graphene. *J. Phys. Chem. Lett.* **2010**, *1*, 572-580.

12. Pedretti, A.; Villa, L.; Vistoli, G., VEGA - An Open Platform to Develop Chemo-Bio-Informatics Applications, using Plug-In Architecture and Script Programming. *J. Computer-Aided Molec. Des.* **2004**, *18*, 167-173.

13. Stewart, J. J. P., MOPAC2009. *Stewart Computational Chemistry, Colorado Springs, CO, USA,* http://openmopac.net/ 2008.

14. Phillips, J. C.; Braun, R.; Wang, W.; Gumbart, J.; Tajkhorshid, E.; Villa, E.; Chipot, C.; Skeel, R. D.; Kale, L.; Schulten, K., Scalable Molecular Dynamics with NAMD. *J. Computational Chem.* **2005**, *26*, 1781-1802.